Nanoscale Res Lett (2009) 4:839–845
DOI 10.1007/s11671-009-9322-x

NANO EXPRESS

Magnetic and Cytotoxicity Properties of $La_{1-x}Sr_xMnO_3$ ($0 \leq x \leq 0.5$) Nanoparticles Prepared by a Simple Thermal Hydro-Decomposition

Sujittra Daengsakul · Chunpen Thomas · Ian Thomas · Charusporn Mongkolkachit · Sineenat Siri · Vittaya Amornkitbamrung · Santi Maensiri

Received: 23 December 2008 / Accepted: 14 April 2009 / Published online: 9 May 2009

Abstract This study reports the magnetic and cytotoxicity properties of magnetic nanoparticles of $La_{1-x}Sr_xMnO_3$ (LSMO) with $x = 0$, 0.1, 0.2, 0.3, 0.4, and 0.5 by a simple thermal decomposition method by using acetate salts of La, Sr, and Mn as starting materials in aqueous solution. To obtain the LSMO nanoparticles, thermal decomposition of the precursor was carried out at the temperatures of 600, 700, 800, and 900 °C for 6 h. The synthesized LSMO nanoparticles were characterized by XRD, FT-IR, TEM, and SEM. Structural characterization shows that the prepared particles consist of two phases of $LaMnO_3$ (LMO) and LSMO with crystallite sizes ranging from 20 nm to 87 nm. All the prepared samples have a perovskite structure with transformation from cubic to rhombohedral at thermal decomposition temperature higher than 900 °C in LSMO samples of $x \leq 0.3$. Basic magnetic characteristics such as saturated magnetization (M_S) and coercive field (H_C) were evaluated by vibrating sample magnetometry at room temperature (20 °C). The samples show paramagnetic behavior for all the samples with $x = 0$ or LMO, and a superparamagnetic behavior for the other samples having M_S values of ~20–47 emu/g and the H_C values of ~10–40 Oe, depending on the crystallite size and thermal decomposition temperature. Cytotoxicity of the synthesized LSMO nanoparticles was also evaluated with NIH 3T3 cells and the result shows that the synthesized nanoparticles were not toxic to the cells as determined from cell viability in response to the liquid extract of LSMO nanoparticles.

Keywords Manganite · Nanoparticles · Synthesis · X-ray diffraction · Magnetic properties · Electron microscopy · Cytotoxicity

S. Daengsakul · C. Thomas · I. Thomas · V. Amornkitbamrung · S. Maensiri (✉)
Department of Physics, Faculty of Science, Khon Kaen University, Khon Kaen 40002, Thailand
e-mail: sanmae@kku.ac.th; santimaensiri@gmail.com

S. Daengsakul · C. Thomas · I. Thomas · S. Siri · V. Amornkitbamrung · S. Maensiri
Integrated Nanotechnology Research Center (INRC), Khon Kaen University, Khon Kaen 40002, Thailand

C. Mongkolkachit
National Metal and Materials Technology Center (MTEC), 114 Thailand Science Park, Paholyothin, Klong Luang, Pathumthan 12120, Thailand

S. Siri
Department of Biochemistry, Faculty of Science, Khon Kaen University, Khon Kaen 40002, Thailand

Introduction

The perovskite manganites $La_{1-x}Sr_xMnO_3$ have recently attracted much attention because of their technical applications [1, 2]. Sr-doped $LaMnO_3$ or LSMO is particularly of interest due to its good magnetic, electrical, and catalytic properties and nowadays is increasingly becoming an attractive possibility in several biomedical applications. A variety of methods has been attempted for the preparation of highly homogeneous and fine powders of these perovskite manganites, including the citrate-gel process [3], sol–gel route [4], molten salt method [5], autocombustion process [6], and hydrothermal synthesis [7], to name just a few. Among these established synthesis methods, it is still critical to find simple and cost effective routes to synthesize LSMO nanocrystalline with a well controlled, reproducible, and narrow size distribution of ferromagnetic nanoparticles with large magnetic moment per particle by

utilization of cheap, nontoxic, and environmentally benign precursors.

In this paper, we report a simple and cost effective synthesis of $La_{1-x}Sr_xMnO_3$ nanoparticles with $x = 0$, 0.1, 0.2, 0.3, 0.4, 0.5 by using the decomposition mechanism of metal acetate salts in water at various temperatures of 600–900 °C. The influence of Sr concentration on the structure and the morphology of the samples was characterized by XRD, FT-IR, SEM, and TEM. Magnetic properties of the samples were investigated by vibrating sample magnetometer (VSM). The effects of Sr concentration and thermal decomposition temperature on the magnetic properties were also discussed in detail. The last part of the investigation concerns the result of cytotoxicity testing of the synthesized sample by MTT assay.

Experimental Details

Magnetic nanoparticles of $La_{1-x}Sr_xMnO_3$ (LSMO) with $x = 0$, 0.1, 0.2, 0.3, 0.4, 0.5 were prepared via the thermal hydro-decomposition method. In this process, high purity acetates of $La(CH_3COO)_3 \cdot xH_2O$ (99.9%, Aldrich), $Mn(CH_3COO)_2 \cdot 4H_2O$ (>99.9%, Fluka), and $Sr(CH_3COO)_2$ (99%, Aldrich) were used as starting materials. In a typical procedure, 0.007 mol metal acetates with a mole ratio corresponding to the nominal composition of La: Sr: Mn ratio of 1−x: x: 1 were dissolved in deionized water (DI water) at a ratio of 5:1 (volume/weight) of DI water to total acetate salts. The mixed solution was stirred with a magnetic stirrer at room temperature for 15 min, and was thermally decomposed in an oven under normal atmosphere at different temperatures of 600, 700, 800, and 900 °C for 6 h and left to cool down to room temperature before being ground to obtain LSMO nanoparticles.

The crystal structure of the synthesized LSMO nanoparticles was characterized by X-ray diffraction (XRD) (Philips PW3040, The Netherlands) with the crystallite size calculated from the broadening of the XRD peaks using Debye–Scherrer method. The functional groups present in the samples were studied using the Fourier Transform Infrared Spectroscopy technique (FT-IR) (Spectrum one, Perkin Elmer Instrument, USA). The samples were incorporated in KBr pellets for which the FT-IR spectra were obtained in the 1000–450 cm^{-1} wave-number range. The morphology of the samples was revealed by scanning electron microscopy (SEM) (LEO 1450VP, UK) and transmission electron microscopy (TEM) (JEOL 2010, 200 kV, Japan). The selected area electron diffraction (SAED) patterns from TEM and high resolution TEM (HRTEM) images were analyzed to identify the phase and crystal structure, and to confirm the results obtained from XRD. The magnetic properties were investigated by Vibrating Sample Magnetometer (VSM) (Lakeshore 7403, USA) at room temperature (20 °C).

The cytotoxicity of LSMO nanoparticles was evaluated with NIH 3T3 and cell viability was determined by MTT colorimetric assay (Sigma, USA). Cells were seeded on the 96-well culture plate (1×10^4 cells/well) for 24 h. The extracted LSMO liquid was taken by boiling LSMO particles in sterile distilled water at 121 °C for 1 h with concentration of 0.2 g/mL. Cells were incubated with 20 mL extracted LSMO liquid or sterile water (control) for 24 h. After removing the medium, 10 mL of 12 mM MTT solution was added and incubated for a further 4 h. Blue formazan crystals, metabolized MTT in mitochondria of viable cells, were dissolved in 50 mL of dimethylsulfoxide (DMSO; Sigma, USA) and measured at 550 nm by the plate reader (Biorad, Japan). The average value of four wells was used for each sample and two repeats were done in each experiment. The control NIH 3T3 cell viability was defined as 100%. Statistical comparison was performed using one-way ANOVA with SPSS software version 11.5 (SPSS, Germany).

Results and Discussion

Structural and Morphology Characterization

The XRD results of the prepared LSMO nanoparticles at 600, 700, 800, and 900 °C for 6 h are shown in Fig. 1. For LSMO samples prepared at 600 °C (Fig. 1a), the perovskite structures are seen to be dominant in the samples with $0.1 \leq x \leq 0.3$ while the others show many impurity phases such as La_2O_3, La_2CO_3OH, $La(OH)_3$, and $SrCO_3$. The earlier formation of perovskite phase when there was a small doping of Sr ($x < 0.3$) into the LMO structure compared with an undoped sample ($x = 0$) at 600 °C indicates that Sr substitution for La can help stabilize the oxide phase at lower temperature. This phenomenon agrees with the one found by Gaudon et al. [4] for LSMO prepared by sol–gel method, while for the samples with $x > 0.3$, the substitution of Sr cannot help perovskite phase formation as well as for a small doping since impurity phases of $SrCO_3$ and $La(OH)_3$ are more observed. This result may be because there is a limit to the incorporation of Sr for $LaMnO_3$ lattice which affects the formation of the LSMO perovskite phase. For the samples annealed at higher temperatures (Fig. 1b–d), the peaks due to LSMO perovskite phase show stronger and sharper profiles resulting from the continuation of crystallization process and gradual grain growth [8]. Each XRD peak of samples with $x \leq 0.3$ splits into well-resolved peaks, which is in accordance to the cubic symmetry reduction and changing

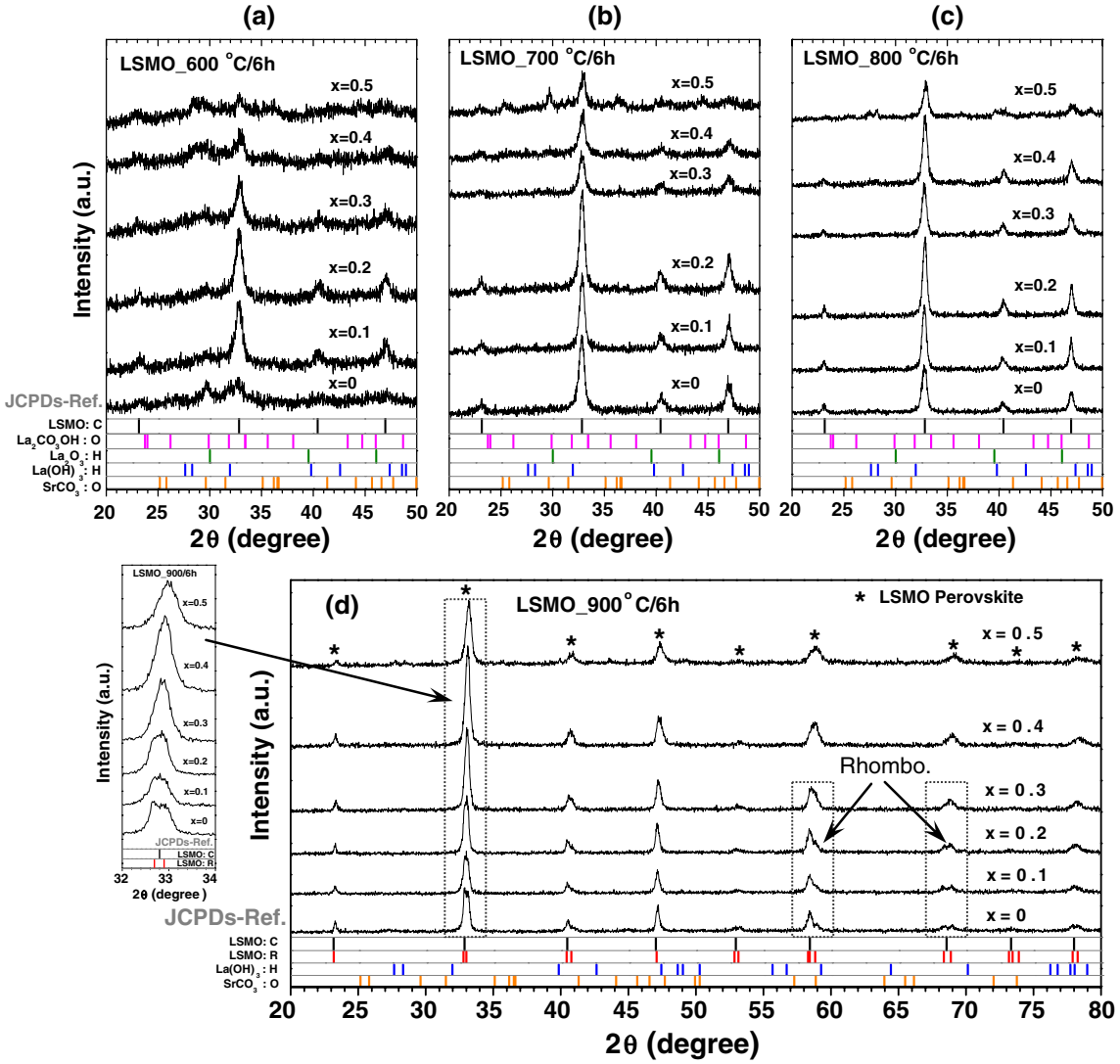

Fig. 1 XRD spectra of LSMO nanoparticles with $0 \leq x \leq 0.5$ thermally decomposed at **a** 600 °C, **b** 700 °C, **c** 800 °C, and **d** 900 °C for 6 h

to rhombohedral of this perovskite. This crystal structure transformation occurs at 900 °C in most samples except for $x > 0.3$. These results are in good agreement with the work reported by Gaudon et al. [4]. The substitution of divalent cation Sr^{2+} for trivalent cation La^{3+} site in $LaMnO_3$ perovskite can induce the formation of Mn^{4+} ion. However, the content of Mn^{4+} ions is fixed not only by substituting Sr^{2+} for La^{3+} site, but also by creation of cation vacancies or non-stoichiometry ($La_{1-x}Sr_xMnO_{3+\delta}$) which depends on firing atmosphere, temperature, time, and also on the preparation procedure [9, 10]. Therefore, the substitution of smaller radii ions of Mn^{4+} for some larger radii ions of Mn^{3+} leads to distortion of the perovskite structure which easily occurs in the samples with $x \leq 0.3$. This is because the ability to form over stoichiometric of LSMO compounds in air decreases with increasing Sr concentration and mostly disappears at $x > 0.3$ [4, 10]. Thus, the crystal transformation for these prepared samples with $x \leq 0.3$ may be due to lattice distortion caused by higher Mn^{4+} ion content.

The crystallite sizes of the synthesized samples were determined from XRD line-broadening of the largest intensity for a single peak at $2\theta^\circ \approx 47^\circ$ using the Debye-Scherrer equation. The obtained crystallite sizes as function of the thermally decomposed temperature for the samples with $0 \leq x \leq 0.5$ are listed in Table 1 and also displayed in Fig. 2. It is clearly seen that the crystallite size increases with increasing thermal decomposition temperature and decreases with the increase of Sr content.

Figure 3 shows the FT-IR spectra of the samples prepared at 600 and 900 °C for 6 h. The main absorption band around 600 cm^{-1} corresponds to stretching of the metal–oxygen bond in the perovskite, which involves the internal motion of a change in Mn–O–Mn bond length in MnO_6

Table 1 Properties of prepared LSMO

$La_{1-x}Sr_xMnO_3$	Thermally decomposed in the range of 700 → 900°C for 6 h					
Sr content	0	0.1	0.2	0.3	0.4	0.5
Crystal structure	Cubic → Rhombo	Cubic → Rhombo	Cubic → Rhombo	Cubic → Rhombo	Cubic	Cubic
Crystallite size (nm)	20–62	23–48	21–53	16–40	14–29	9–29
Magnetization (emu/g)	–	10.4–27.9	15.2–40.4	9.9–46.8	5.0–38.1	1.3–20.4
Coercivity (Oe)	–	3.6–17.5	7.5–33.3	8.6–39.4	7.3–35.9	6.9–30.5

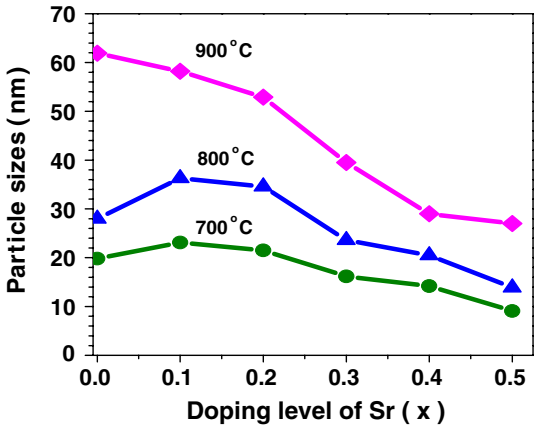

Fig. 2 Particle size of LSMO nanoparticles with $0 \leq x \leq 0.5$ thermally decomposed at 700–900 °C for 6 h

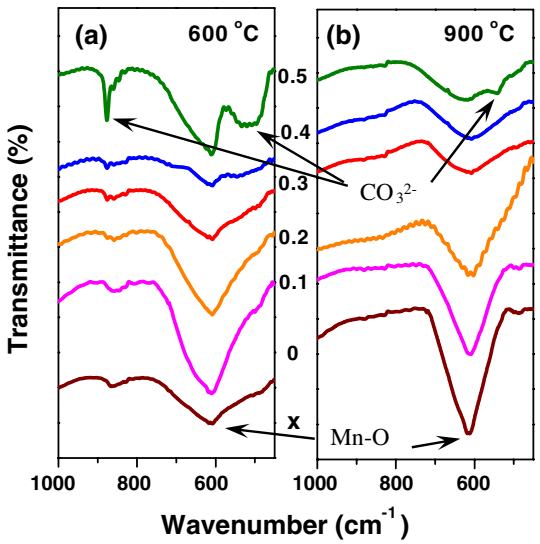

Fig. 3 FTIR spectra of the LSMO nanoparticles with $0 \leq x \leq 0.5$ thermally decomposed for 6 h at **a** 600 °C and **b** 900 °C

octahedral [11]. For all of the samples prepared at 600 °C, the presence of an absorption band of CO_3^{2-} functional group at around 860–900 cm^{-1} was observed. These bands correspond to the impurity phase of $SrCO_3$ or La_2CO_3OH which disappears at higher temperature of thermal decomposition except in the case of $x = 0.5$. The FT-IR results agree well with the results of XRD (Fig. 1).

The detailed morphologies of the prepared samples for all x values at 900 °C, revealed by SEM and TEM, are shown in Figs. 4 and 5, respectively. The SEM images reveal that the prepared samples are spherical consisting of agglomerated nanoparticles with particle sizes of ca. 50–100 nm. Clear morphology can be seen via TEM images showing the particle sizes in the range of 30–80 nm. It is clearly seen from the TEM images that the particle size decreases with increasing Sr concentration. This is in good agreement with the results estimated from XRD line-broadening (Table 1 and Fig. 2). The corresponding SAED patterns, given as insets in Fig. 5, show spotty ring patterns suggesting a polycrystalline structure in all the prepared LSMO samples. The observation of lattice fringes of the rhombohedral structure of LSMO phase in the samples for $x = 0.1$ and 0.2 from HRTEM (insets in Fig. 5) also confirms the transformation of crystal structure from cubic to rhombohedral in the 900 °C-prepared samples with $x < 0.3$.

Magnetic Characterization

The specific magnetization (M_S) curves obtained from VSM measurements shown in Fig. 6 indicate superparamagnetic behavior for all the samples thermally decomposed at 600–900 °C except for the LMO ($x = 0$) samples which are paramagnetic. It is seen from Fig. 6 that the magnetic saturation depends on both the Sr concentration and thermal decomposition temperature. The slopes of the M–H curves in the range from 3 kOe to 10 kOe for the samples with x values of 0.1 and 0.2 are equal to those of $x = 0$ (LMO), indicating the presence of paramagnetic phases of LMO contamination in the samples with $x = 0.1$ and 0.2. The M_S value increases as the Sr content increases and shows the highest value at $x = 0.3$ and then decreases as x increases to 0.5. These results indicate that the sample with $x = 0.3$ has the most appropriate Mn^{4+} ion content ($Mn^{4+}/Mn^{3+} \approx 1$) for the double exchange interaction

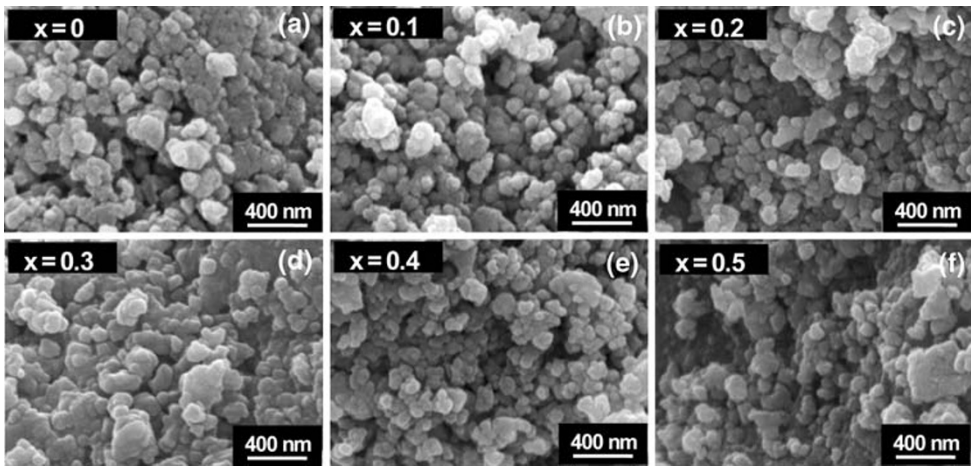

Fig. 4 SEM micrographs of the LSMO nanoparticles with $0 \leq x \leq 0.5$ thermally decomposed at 900 °C for 6 h

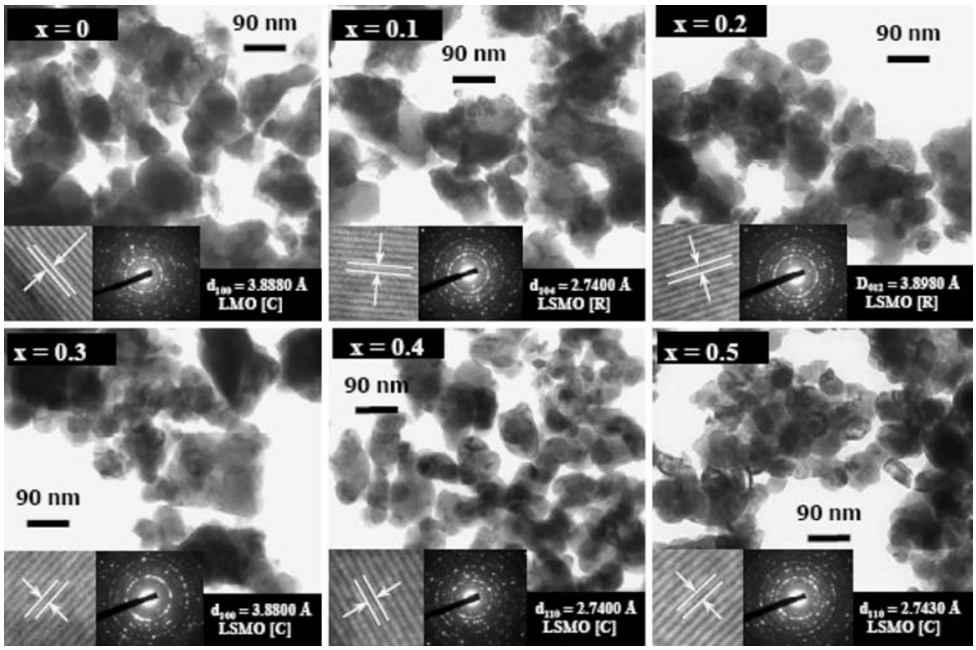

Fig. 5 TEM images with corresponding SAED patterns and lattice fringes from HRTEM of the LSMO nanoparticles with $0 \leq x \leq 0.5$ thermally decomposed at 900 °C for 6 h

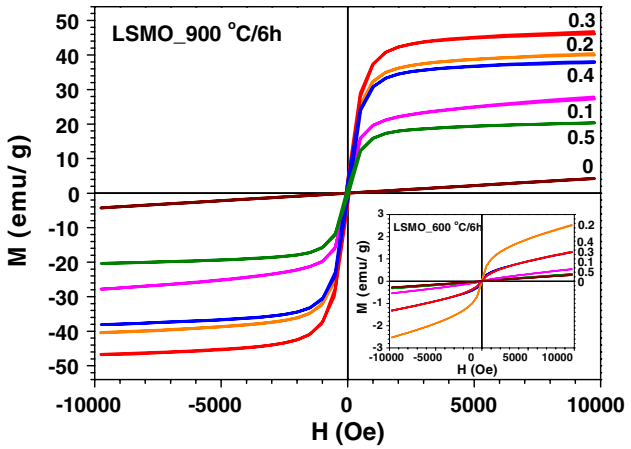

Fig. 6 Room temperature M vs. H of the LSMO nanoparticles with $0 \leq x \leq 0.5$ thermally decomposed at 900 °C for 6 h (inset is the data for samples thermally decomposed at 600 °C)

(Mn^{4+}–O–Mn^{3+}) while the other samples have more pairs of ions Mn^{3+}–O–Mn^{3+}($x < 0.3$) or Mn^{4+}–O–Mn^{4+} ($x > 0.3$), which result in less double exchange interactions and thus a reduction in M_S.

Figure 7 shows M_S of the samples as a function of thermal decomposition temperature. The samples with $x \leq 0.2$ show a linear relationship between M_S and preparation temperature. For the sample with $x \geq 0.3$, there is a rapid increase of M_S when the decomposition temperature is above 700 °C. This may be due to (i) the substitution of Sr^{2+} for La^{3+} which leads to an increase in the Mn^{4+} content which favors the double exchange interaction, and (ii) the higher Curie temperature (T_C) values of the samples with $x \geq 0.3$ samples than those of the samples with $x < 0.3$ [5]. At the decomposition temperatures below 900 °C, the M_S value increases with increasing Sr content and reaches the highest value of

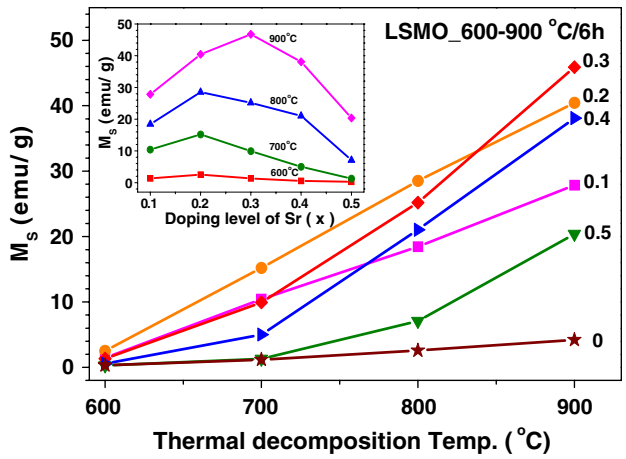

Fig. 7 M_S of the LSMO nanoparticles with $0 \leq x \leq 0.5$ as a function of thermal decomposition temperatures of 600–900 °C (inset is the relationship between M_S and Sr concentrations)

40.4 emu/g for the samples with $x = 0.2$ (inset in Fig. 7). The 900 °C-prepared sample with $x = 0.3$ shows the highest M_S value of 46.8 emu/g. This value is comparable to the value of 45 emu/g for $La_{0.7}Sr_{0.3}MnO_3$ nanoparticles (~30 nm) synthesized by citrate-gel route reported by Rajagopal et al. [12], and higher than the value of 23 emu/g for $La_{0.7}Sr_{0.3}MnO_3$ nanoparticles (~48 nm) synthesized by sol–gel route reported by Duan et al. [13]. The properties of the prepared samples in this study are summarized in Table 1.

Cytotoxicity

The results of cytotoxicity test of the LSMO nanoparticles with $0.2 \leq x \leq 0.4$ prepared at the temperature conditions of 600, 700, 800, and 900 °C are shown in Fig. 8. The results indicated that the prepared LSMO nanoparticles were quite less toxic to the cells. Cell viability in response to the liquid extraction of LSMO nanoparticles ranged from 91.3% to 98.2% (Fig. 8). The Sr amounts or the decomposition temperatures were not clearly related to the cytotoxicity of the nanoparticles to the tested cells. Therefore, further work is needed to clarify this point.

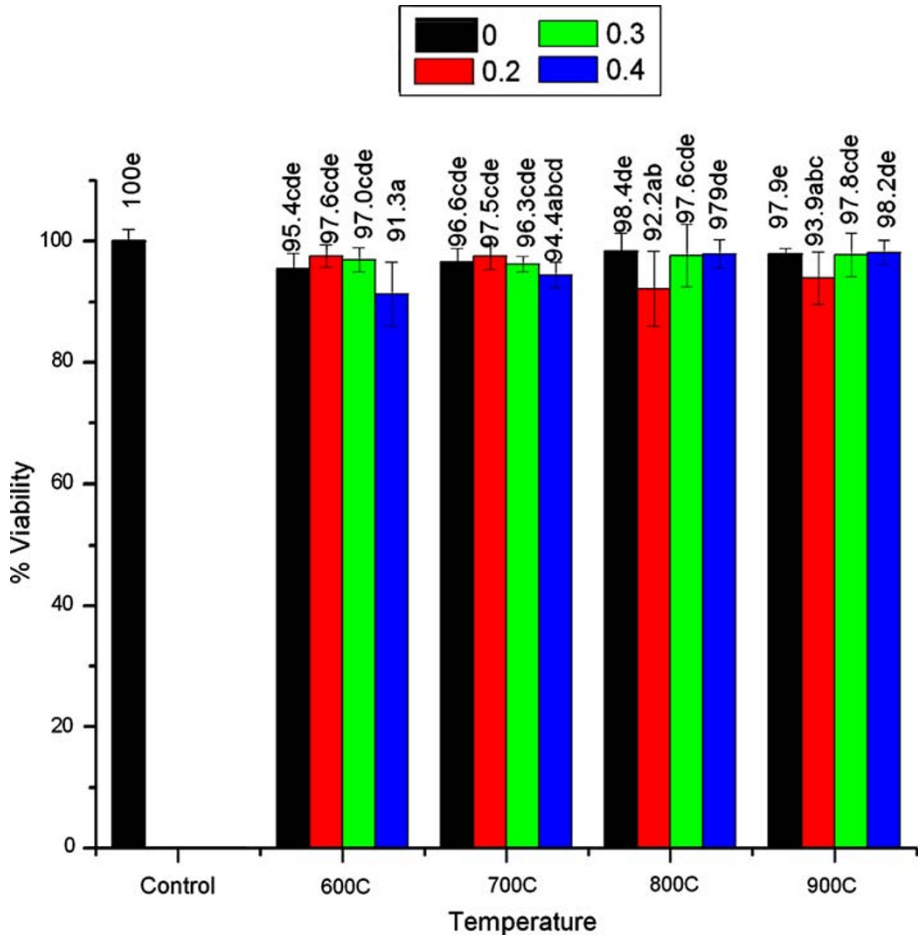

Fig. 8 Cytotoxcity of LSMO nanoparticles with $0.2 \leq x \leq 0.4$ at the temperature conditions of 600, 700, 800, and 900 °C was studied on NIH 3T3 cells. Cells were incubated with the liquid extractions of nanoparticles or water (control) for 24 h before cell viability was determined by MTT assay

Conclusions

LSMO nanoparticles with $0 \leq x \leq 0.5$ have been synthesized by a simple thermal decomposition method using acetate salts in DI water. Structural characterization shows that the structure transforms from cubic to rhombohedral in the prepared samples with $x \leq 0.3$ when decomposed at 900 °C, while the others remained cubic in structure. Study of magnetic properties at room temperature shows that M_S depends strongly on the thermal decomposition temperature for samples of $x \geq 0.2$, and has no exact dependence on Sr concentration. There is a variation of M_S with Sr content with the maximum at $x = 0.3$ for decomposition temperature of 900 °C, and at temperature below this the maximum M_S of 40.4 emu/g is found at $x = 0.2$. In addition, the magnetic nanoparticles show no toxicity to the tested cells, NIH 3T3, as determined from the result of cell viability in response to the liquid extraction of the magnetic nanoparticles. This will be useful for medical applications. The present work has shown that the thermal hydro-decomposition is a new useful method for preparation of manganite nanoparticles, and gives a potential avenue for further practical scale-up of the production process and applications.

Acknowledgments The authors would like to thank the Department of Chemistry of Khon Kaen University for providing FT-IR and VSM facilities, the Faculty of Science Electron Microscopy Unit for providing SEM facilities, and the National Metal and Materials Technology Center (MTEC) of NSTDA for providing TEM facilities. S. Daengsakul would like to thank the TGIST scholarship for the support of her Ph.D. study. This work is financially supported by The National Research Council of Thailand (NRCT) under the research contract no. PorKor/2550-287.

References

1. J. Heremans, J. Phys. D Appl. Phys. **26**, 1149 (1993). doi:10.1088/0022-3727/26/8/001
2. K. Dorr, J. Phys. D Appl. Phys. **39**, R125 (2006). doi:10.1088/0022-3727/39/7/R01
3. N.D. Lipham, G.M. Tsoi, L.E. Wenger, IEEE Trans. Magn. **43**, 3088 (2007). doi:10.1109/TMAG.2007.893850
4. M. Gaudon, C. Laberty-Robert, F. Ansart, P. Stevens, A. Rousset, Solid State Sci. **4**, 125 (2002). doi:10.1016/S1293-2558(01)01208-0
5. Y. Tain, D. Chen, X. Jiao, Chem. Mater. **18**, 6088 (2006). doi:10.1021/cm0622349
6. B.M. Nagabhushana, R.P. Sreekanth Chakradhar, K.P. Ramesh, C. Shivakumara, G.T. Chandrappa, Mater. Res. Bull. **41**, 1735 (2006). doi:10.1016/j.materresbull.2006.02.014
7. C. Li, T. Li, B. Wang, H. Yan, J. Cryst. Growth **295**, 137 (2006). doi:10.1016/j.jcrysgro.2006.06.005
8. S. Mathur, H. Shen, J. Sol–Gel Sci. Technol. **25**, 147 (2002)
9. J. Töpfer, J.B. Goodenough, J. Solid State Chem. **130**, 117 (1997). doi:10.1006/jssc.1997.7287
10. J.H. Kuo, H.U. Anderson, D.M. Sparlin, J. Solid State Chem. **83**, 52 (1989). doi:10.1016/0022-4596(89)90053-4
11. F. Gao, R.A. Lewis, X.L. Wang, S.X. Dou, J. Alloy Comp. **347**, 314 (2002). doi:10.1016/S0925-8388(02)00789-2
12. R. Rajagopal, J. Mona, S.N. Kale, T. Bala, R. Pasricha, P. Poddar, M. Sastry, B.L.V. Prasad, D.C. Kundaliya, S.B. Ogale, Appl. Phys. Lett. **89**, 023107 (2006). doi:10.1063/1.2210080
13. Y.W. Duan, X.L. Kou, J.G. Li, Physica B **355**, 250 (2005). doi:10.1016/j.physb.2004.10.100